Research Article | Vol. 27, No. 2 | 21 Jan 2019 | OPTICS EXPRESS 1488
Optics EXPRESS

Comparative study of Yb:KYW planar waveguide lasers Q-switched by direct- and evanescent-field interaction with carbon nanotubes

JUN WAN KIM,[1] SUN YOUNG CHOI,[2] JI EUN BAE,[2] MI HYE KIM,[3] YOUNG UK JEONG,[3] ESROM KIFLE,[4] XAVIER MATEOS,[4] MAGDALENA AGUILÓ,[4] FRANCESC DÍAZ,[4] UWE GRIEBNER,[5] VALENTIN PETROV,[5] GUANG-HOON KIM,[1] AND FABIAN ROTERMUND[2,*]

[1]*Medical Device Research Center, Korea Electrotechnology Research Institute (KERI), 15588 Ansan, South Korea*
[2]*Department of Physics, Korea Advanced Institute of Science and Technology (KAIST), 34141 Daejeon, South Korea*
[3]*Radiation Center for Ultrafast Science, Korea Atomic Energy Research Institute (KAERI), 34057 Daejeon, South Korea*
[4]*Física i Cristal·lografía de Materials i Nanomaterials (FiCMA-FiCNA), Universitat Rovira i Virgili (URV), 43007 Tarragona, Spain*
[5]*Max Born Institute for Nonlinear Optics and Short Pulse Spectroscopy, 12489 Berlin, Germany*
[*]*rotermund@kaist.ac.kr*

Abstract: Both direct- and evanescent-field interactions with carbon nanotubes (CNTs) are applied to achieve stable Q-switched operation of Yb:KYW planar waveguide lasers. The performance characteristics were investigated in a same cavity configuration and analyzed in detail in the following three cases, CNTs deposited onto end mirror (M-coating), output coupler (OC-coating) and top surface of the planar waveguide (WG-coating). Maximum output powers, repetition rates, and minimum pulse durations are 61 mW, 1103 kHz and 215 ns for OC-coating, 39 mW, 1052 kHz and 275 ns for WG-coating, and 26 mW, 1119 kHz and 217 ns for M-coating, respectively. From the calculation of the configuration-dependent stability range, the beam size and the electric field distribution in the Yb:KYW planar waveguide, it is confirmed that the evanescent-field interaction scheme makes stable Q-switching possible with much lower intensities at saturable absorber compared to the direct-field interaction scheme in the presented waveguide laser operation.

1. Introduction

Compact pulsed lasers are widely used in medical and biological applications, nonlinear spectroscopy, machining, frequency comb generation, and communications [1–6]. One of the most compact pulsed laser formats is the waveguide laser. It turned out to be a promising solution due to its simplicity, miniaturization, low pump power requirements, and cost-effectiveness. In addition, it provides a great potential for future on-chip integrated pulsed light sources. Recently, numerous approaches have been demonstrated based on different waveguide structures with diverse gain media and saturable absorbers (SAs) [7–20].

The Yb^{3+}-doped gain media have been developed and widely used for efficient bulk solid-state laser operation in continuous-wave (cw) and pulsed regimes. The small quantum defect reduces the thermal load and increases the laser efficiency due to the spectral neighborhood of absorption and emission with very large cross sections and the absence of alternative paths for depopulation by excited-state absorption or energy-transfer up-conversion. Furthermore, the relatively long upper-state lifetime is beneficial for Q-switched operation. Meanwhile, the

#348227 https://doi.org/10.1364/OE.27.001488
Journal © 2019 Received 22 Oct 2018; revised 28 Dec 2018; accepted 28 Dec 2018; published 16 Jan 2019

Optics EXPRESS

rare-earth ion-doped monoclinic double-tungstate host material $KY(WO_4)_2$ (KYW), which exhibits large refractive indices, high third-order nonlinearity, large absorption and emission cross section, broad linewidths and minimal quenching effects, has been investigated for bulk and waveguide amplification [20]. Thanks to the superior characteristics of Yb:KYW and the waveguide geometry, Yb:KYW planar waveguide lasers operating near 1 μm have been successfully demonstrated in the cw and pulsed regimes [10,11,21]. However, the low refractive index contrast due to the low doping concentration of the active ions sometimes leads to a relatively thick planar waveguide. This thick planar waveguide structure may lead to low beam intensity and multimode operation in the waveguide. To overcome such a low refractive index contrast, Gd^{3+} and Lu^{3+} co-doped KYW host materials have been proposed and widely investigated [22–26]. By substituting the low electron density ions of Y^{3+} for the higher electron density ions of Gd^{3+} and Lu^{3+}, refractive index contrast can increase while maintaining the doping ratio of active ions.

Saturable absorbers (SAs) applicable as passive optical switching devices are commonly used to realize more compact pulsed waveguide lasers. However, most SAs employed in waveguide lasers suffer from the damage problem due to the small beam size corresponding to the waveguide scale. To overcome this issue, the evanescent-field interaction scheme with bis(4-dimethylaminodithiobenzil)nickel (BDN) dye as SA deposited on top of waveguides was proposed [8,9]. Due to the low intensity of an evanescent-field at the SA, this scheme does not only avoid the optical damage and thermal problems of the SA, but is also suitable for a compact and integrated pulsed laser source, because the position of the SA does not disturb the cavity configuration. Recently, evanescent field interactions with SAs based on carbon nanotubes (CNTs) and 2D materials such graphene, tungsten disulfide (WS_2) and black phosphorous in waveguide lasers have been investigated [10–16]. However, most studies report the performance of the specific pulsed laser itself and comparative analysis of the direct- and evanescent-field interaction schemes has not been carried out, yet.

In this work, we investigated both evanescent-field and direct-field interaction schemes of the Q-switched Yb:KYW planar waveguide laser for a comparative study. CNTs are used as SAs, since they can be easily integrated at different positions, and their properties including linear and nonsaturable losses and modulation depth are precisely controllable. In the same cavity configuration, CNT-SAs are positioned on the HR-end mirror (M-coating) and output coupler (OC-coating) for direct-field interaction, respectively, and on the top surface of the Yb:KYW planar waveguide (WG-coating) for evanescent-field interaction. All configurations show stable Q-switched operation with typical tendencies for a saturable absorber Q-switched laser. Based on the calculation of the beam mode and the amplitude ratio of the electric field distribution within the Yb:KYW planar waveguide, maximum intensities at the SA in each case are compared. It turned out that the maximum intensity at the SA for the WG-coating is about 1500 times lower than that for the M-coating case.

2. Fabrication of waveguide and CNT-SAs

The Yb:KYW planar waveguide was fabricated by the liquid phase epitaxy (LPE) method as described in [26,27]. First, the undoped KYW substrate was grown by the top-seeded solution growth (TSSG) slow-cooling method. It was cut parallel to the (010) natural face and polished to laser grade quality. The active layer with a composition of $KY_{0.59}Gd_{0.185}Lu_{0.21}Yb_{0.015}(WO_4)_2$ (1.5 at.% Yb) was grown by LPE from a solution with solute/solvent ratio of 7/93 mol%. The precursors used were Y_2O_3, Gd_2O_3, Lu_2O_3, Yb_2O_3, WO_3, and K_2CO_3. Potassium ditungstate, $K_2W_2O_7$, was used as a solvent. In this case, Gd^{3+} and Lu^{3+} ions were co-doped to reduce the lattice mismatch, increase the refractive index difference and decrease the thickness of planar waveguide, because Gd^{3+} and Lu^{3+} exhibit large atomic numbers compared to Y^{3+}. Subsequently, the cleaned 2-mm-thick KYW substrate was vertically dipped into the solution, rotating it at 10 rpm. Once the growth process was completed, the sample was slowly extracted, fixed 3 mm above the solution and

Optics EXPRESS

cooled to room-temperature at a rate of 1.5 K/h to avoid any cracks and thermal stress between the substrate and the epilayer. At this time, we did not deposit a top-cladding-layer on the planar waveguide. The lateral side was cut perpendicular to the N_g axis of the beam propagation direction and each end facet and top surface of the planar waveguide were polished to laser quality. After polishing and cutting, we prepared a 10.7-μm-thick, 5.75-mm-long Yb:KYW planar waveguide. The overall loss arising from coupling, absorption and other propagation losses through the waveguide was measured to be about 0.95 dB.

The fabrication process of CNT-SAs follows the one described in [28]. CNTs synthesized by the arc-discharge method exhibiting broadband absorption around 1 μm are chosen as starting material. These CNTs are dissolved in 1,2-dichlorobenzene (DCB) and the well-dispersed upper portion of CNTs is extracted after centrifugation. The CNT-DCB solution is then mixed with poly(methyl methacrylate) (PMMA). The prepared CNT/PMMA mixture in DCB is finally spin-coated on output coupler, end mirror and top surface of the waveguide. Subsequently, the SA layers were dried on a hot plate. To characterize saturable absorption properties of CNTs such as saturation fluence, modulation depths and nonsaturable loss, we performed fluence-dependent nonlinear transmission measurements of CNTs spin-coated on a quartz substrate. Here, the layer thickness and the concentration of CNTs are kept to be same for the case of OC-coating. From this measurement near 1 μm, we extract saturation fluence of 0.65 μJ/cm^2, modulation depth of 0.67% and nonsaturable loss of 0.91%. Note that the coating conditions for each scheme are further optimized to achieve stable Q-switched operation. In the case of waveguide coating, the end facet of the waveguide is protected from the CNT coating to avoid any undesired side effects and disturbances on the laser operation.

3. Experimental results

The schematics of the planar waveguide laser configurations are shown in Fig. 1. A 980-nm single-mode laser diode emitting a maximum cw power of 750 mW (1999 CHP, 3S Photonics) is coupled to a polarization-maintaining fiber and collimator. To prevent possible damages of the laser diode by feedback from the waveguide laser, a Faraday isolator is used. A half-wave plate is placed after the Faraday isolator to match the pump polarization to the N_m-axis of the planar waveguide for the efficient laser operation. Note that the absorption and emission cross sections along the N_m-axis are much larger than those of other axes. To couple the pump beam into the planar waveguide efficiently, two cylindrical lenses with focal lengths of 150 and 30 mm are used. The pump beam size was measured by the knife edge method and the beam waists are 25.48 μm along the x-axis (parallel to the N_m waveguide axis) and 5.07 μm along the y-axis (parallel to the N_p waveguide axis). The latter value is well matched to the thickness of the used waveguide. The output coupler (OC) with 4% transmission at the laser operation wavelength was optimal for a comparative study of Q-switched operation in direct- and evanescent-field interaction schemes. An AR-coated aspheric lens with a focal length of 4.51 mm (C230TME-B, Thorlabs) is inserted between the planar waveguide and OC for compensation of the substantial difference of the beam propagation characteristics between the xz- and yz-planes. In this configuration, the role of the lens in the xz- and yz-planes is different. In the xz-plane, the lens increases the stability region and helps the overlap between the pump and cavity mode for efficient laser operation. In the yz-plane, the lens collimates the divergent beam after the waveguide and re-couples the returned beam to the waveguide.

Optics EXPRESS

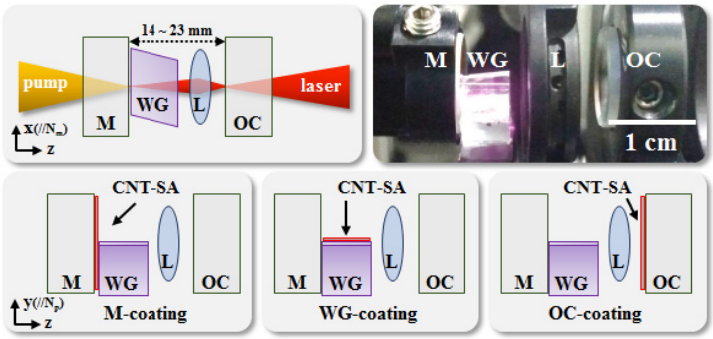

Fig. 1. Schematic of the Yb:KYW planar waveguide laser and CNT-SA positions for M-coating, WG-coating and OC-coating. M, dielectric plane mirror (high transmission at 980 nm and high reflection around 1030 nm); L, aspheric lens with a focal length of f = 4.51 mm; OC, output coupler with 4% transmission.

The output characteristics versus pump power during the stable Q-switched operation are shown in Fig. 2(a). A 4% OC is used in all cases. The maximum output powers for OC-, WG- and M-coating are 61, 39, and 26 mW and the slope efficiency - 12.3%, 9.2% and 6.0%, respectively. The repetition rates versus pump power for OC-, WG- and M-coating are depicted in Fig. 2(b). As the incident pump power increases, the repetition rate also increases from 392 to 1103 kHz for OC-coating, from 414 to 1052 kHz for WG-coating and from 485 to 1119 kHz for M-coating. Figures 2(c) and 2(d) show the dependences of pulse duration and pulse energy zon pump power for the three types of SA coating. The minimum pulse durations and maximum pulse energies are 215 ns and 52 nJ for OC-coating, 275 ns and 35 nJ for WG-coating, and 217 ns and 22 nJ for M-coating. Each case follows the tendencies of the typical fast SA Q-switched lasers [29].

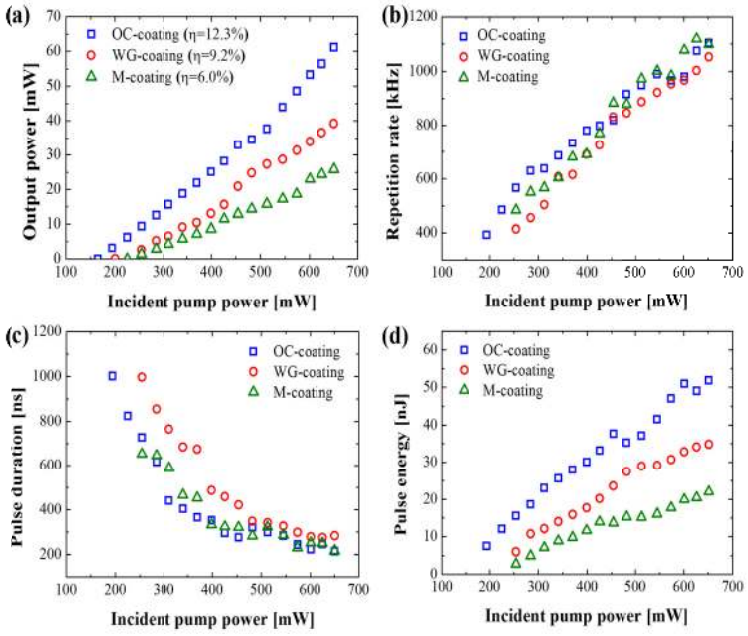

Fig. 2. CNT-SA Q-switched Yb:KYW planar waveguide lasers: (a) output power, (b) repetition rate, (c) pulse duration and (d) pulse energy in the three different SA Q-switched configurations.

Optics EXPRESS

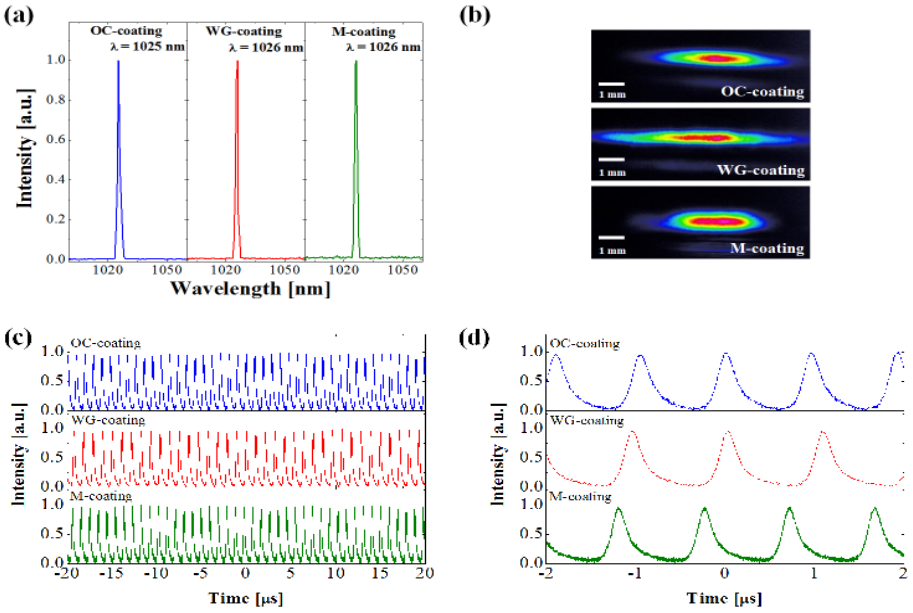

Fig. 3. CNT-SA Q-switched Yb:KYW planar waveguide lasers: (a) spectra, (b) beam profiles and pulse trains measured in different time spans of (c) 40 μs and (d) 4 μs at maximum output powers for the three different SA Q-switched configurations.

The spectrum in stable Q-switched operation for each SA is shown in Fig. 3(a). The center wavelength and spectral bandwidth at FWHM are 1025 nm and 1.3 nm, 1026 nm and 1.4 nm, and 1026 nm and 1.8 nm for OC-, WG-, and M-coating, respectively. The beam profiles shown in Fig. 3(b) are the far-field profiles measured at a distance of 20 cm from OC for the three different cases and closely related to the near-field beam profiles. Along the vertical direction (y-axis), the divergence of the beam is collimated by an intracavity lens, while the beam in the horizontal plane (x-axis) is focused on OC. The difference of the beam profiles is mainly attributed to the cavity-length-dependent x-axis beam size at OC shown in Fig. 4(b). Note that, from the mode number calculation, the waveguide structure allows two modes in the vertical direction, but we could experimentally avoid spatial multi-mode operation by proper selection of the pump beam size and the intracavity lens as well as precise alignments of the lens position and the cavity length. Figures 3(c) and 3(d) show the pulse train measured for each case in different time spans and display stable Q-switched operation.

4. Discussion

To verify the direct-field interaction in the Q-switched Yb:KYW planar waveguide, the maximum intensity at the SA is calculated from the experimental results and the intracavity beam size. Figure 4(a) shows the stability region and the calculated beam size at M and OC. The vertical line denotes the actual cavity length where stable Q-switched operation is achieved in each case. The beam propagation in the xz-plane inside the cavity is shown in Fig. 4(b). As the cavity length decreases, the intracavity beam size in the waveguide increases. From the pulse duration, the pulse energy and the calculated beam size at M and OC, we extract the maximum intracavity peak intensities at SA as ~47 kW/cm^2 for OC-coating and 860 kW/cm^2 for M-coating. The range of cavity length tolerance for Q-switched operation are measured to be 1.2 mm for OC-coating and 8.8 mm for M-coating. This results confirm well the calculated intensities at SA.

Optics EXPRESS

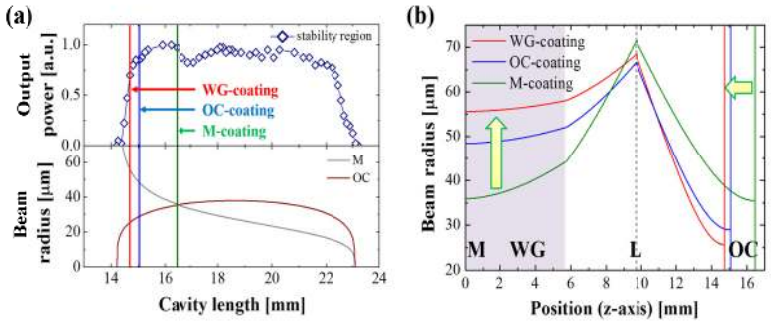

Fig. 4. (a) Measured stability region and intracavity beam size (in x-axis) calculated at the end mirror (M) and output coupler (OC). (b) Calculated beam size in the xz-plane.

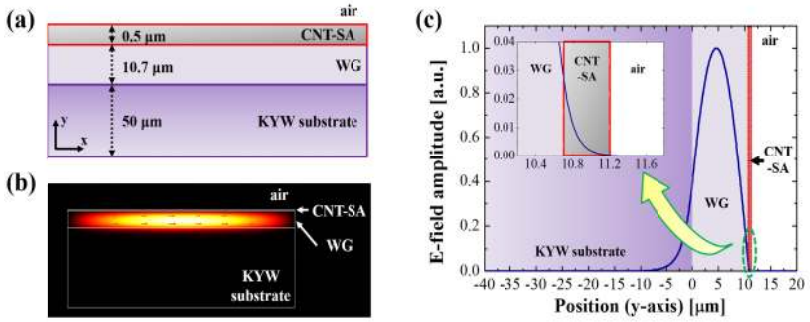

Fig. 5. (a) Structure of the CNT-SA coated Yb:KYW planar waveguide and (b) the calculated electric field distribution of the fundamental guided mode. (c) Calculated electric field amplitude along the y-axis of the Yb:KYW planar waveguide and CNT-SA (inset).

To compare the direct-field interaction scheme with the evanescent-field interaction scheme, the maximum intensities for both interaction schemes have to be considered. We calculate the electric field distribution in our planar waveguide to extract the information of the maximum intensity at the CNT-SA for WG-coating. The structure of the waveguide used in the present work is illustrated in Fig. 5(a). The refractive indices of the CNT-SA layer, Yb:KYW waveguide layer and KYW substrate are assumed to be 1.4817, 2.0879 and 2.0853, respectively [26]. The thickness of each layer is 0.5, 10.7 and 50 μm, respectively, as illustrated in Fig. 5(a). The calculated electric field distribution of the fundamental transverse-electric guided mode is shown in Fig. 5(b). The fundamental mode is confined inside the waveguide showing spatially single mode. Figure 5(c) shows the electric field distribution along the vertical direction in the Yb:KYW planar waveguide and CNT-SA (inset). From the amplitude ratio, we see that the maximum intensity ratio in the CNT-SA is about 0.079% of that in the Yb:KYW planar waveguide. Such a large intensity difference originates from the large refractive index difference between the Yb:KYW planar waveguide and CNT-SA. From this ratio, the maximum intracavity intensity for the evanescent-field interaction scheme is extracted to be 0.56 kW/cm^2, which is about 1500 times lower than that for M-coating. This low intensity is also revealed as the narrow Q-switching inducible range for WG-coating. For the evanescent-field interaction in our laser, a much larger interaction volume is required to compensate for the low interaction intensity. It is effectively complemented by increasing the horizontal beam size in the planar waveguide and the long interaction length of millimeter scale. The results and analysis are summarized in Table 1.

Optics EXPRESS

Table 1. Characteristics of CNT-SA Q-switched Yb:KYW planar waveguide lasers

	OC-coating	WG-coating	M-coating
Pump beam waist	25.48 μm (x-axis) / 5.07 μm (y-axis)		
Output coupler	4% transmission		
Interaction type of SA	Direct field interaction	Evanescent field interaction	Direct field interaction
Maximum output power	61 mW	39 mW	26 mW
Slope efficiency	12.3%	9.2%	6.0%
Repetition rate	392-1103 kHz	414-1052 kHz	485-1119 kHz
Pulse duration	215-1001 ns	275-996 ns	217-654 ns
Center wavelength / FWHM	1025 / 1.3 nm	1026 / 1.4 nm	1026 / 1.8 nm
Cavity length tolerance of *Q*-switching	1.2 mm	Narrow	8.8 mm
Beam size at SA	2.54×10^{-4} cm^2	6.40×10^{-3} cm^2	5.93×10^{-6} cm^2
Maximum intensity at SA (I_{max})	47 kW/cm^2	0.56 kW/cm^2	860 kW/cm^2

The M-coating corresponds to the general direct-field interaction scheme of waveguide lasers because the SA is exposed only to the small beam size corresponding to the waveguide size. Because of the relatively high intensity, the Q-switched operation itself is easily achieved in a broad range of the cavity length tolerance. But stable operation can only be achieved in a narrow range with low output powers due to thermal load due to the relatively high intensity of the pump beam. The OC-coating shows highest output powers among the three different schemes. By controlling the beam parameters via the cavity length, a suitable beam size at the SA with better overlap between the pump and cavity mode is achieved in our cavity configuration. In the case of WG-coating, the output power is higher compared to M-coating with stable Q-switched operation. Because of the lower intensity in the SA, the WG-coating can suppress possible optical and thermal damages efficiently.

5. Conclusion

We demonstrate stable Q-switched operation of Yb:KYW planar waveguide lasers by both direct- and evanescent-field interaction with CNTs. A detailed study is carried out by comparing the maximum intensity at the SA for each operation mode and the laser performance. From the experimental results, and the calculated intracavity beam size and electric field distribution, it is confirmed that the intensity at the SA, required for the evanescent-field interaction, is about 1500 times lower than that of the typical direct-field interaction in the presented waveguide lasers. We believe that this result is meaningful as the first quantitative analysis of evanescent-field interaction scheme in a Q-switched solid-state waveguide laser. In addition, the evanescent-field interaction scheme offers an efficient

Optics EXPRESS

compact solution for pulsed operation of waveguide lasers and can be further applied to various types of waveguide lasers for realization of more compact pulsed lasers.

Funding

National Research Foundation of Korea (2016R1A2A1A05005381, 2017R1A4A1015426); National Research Council of Science & Technology funded by MSIP, Korea (18-12-N0101-41); Spanish Government (MAT 2016-75716-C2-1-R (AEI/FEDER, UE), TEC 2014-55948-R); Generalitat de Catalunya (2017SGR755).

References

1. A. Zajac, M. Skorczakowski, J. Swiderski, and P. Nyga, "Electrooptically Q-switched mid-infrared Er:YAG laser for medical applications," Opt. Express **12**(21), 5125–5130 (2004).
2. R. Aviles-Espinosa, G. Filippidis, C. Hamilton, G. Malcolm, K. J. Weingarten, T. Südmeyer, Y. Barbarin, U. Keller, S. I. Santos, D. Artigas, and P. Loza-Alvarez, "Compact ultrafast semiconductor disk laser: targeting GFP based nonlinear applications in living organisms," Biomed. Opt. Express **2**(4), 739–747 (2011).
3. M. Kuramoto, N. Kitajima, H. Guo, Y. Furushima, M. Ikeda, and H. Yokoyama, "Two-photon fluorescence bioimaging with an all-semiconductor laser picosecond pulse source," Opt. Lett. **32**(18), 2726–2728 (2007).
4. S. Nolte, C. Momma, H. Jacobs, A. Tünnermann, B. N. Chichkov, B. Wellegehausen, and H. Welling, "Ablation of metals by ultrashort laser pulses," J. Opt. Soc. Am. B **14**(10), 2716–2722 (1997).
5. T. M. Fortier, A. Bartels, and S. A. Diddams, "Octave-spanning Ti:sapphire laser with a repetition rate >1 ghz for optical frequency measurements and comparisons," Opt. Lett. **31**(7), 1011–1013 (2006).
6. X. Sun, D. R. Skillman, E. D. Hoffman, D. Mao, J. F. McGarry, L. McIntire, R. S. Zellar, F. M. Davidson, W. H. Fong, M. A. Krainak, G. A. Neumann, M. T. Zuber, and D. E. Smith, "Free space laser communication experiments from Earth to the Lunar Reconnaissance Orbiter in lunar orbit," Opt. Express **21**(2), 1865–1871 (2013).
7. A. Choudhary, A. A. Lagatsky, P. Kannan, W. Sibbett, C. T. A. Brown, and D. P. Shepherd, "Diode-pumped femtosecond solid-state waveguide laser with a 4.9 GHz pulse repetition rate," Opt. Lett. **37**(21), 4416–4418 (2012).
8. R. Salas-Montiel, L. Bastard, G. Grosa, and J.-E. Broquin, "Hybrid Neodymium-doped passively Q-switched waveguide laser," Mater. Sci. Eng. B **149**(2), 181–184 (2008).
9. B. Charlet, L. Bastard, and J. E. Broquin, "1 kW peak power passively Q-switched Nd^{3+}-doped glass integrated waveguide laser," Opt. Lett. **36**(11), 1987–1989 (2011).
10. J. W. Kim, S. Y. Choi, D.-I. Yeom, S. Aravazhi, M. Pollnau, U. Griebner, V. Petrov, and F. Rotermund, "Yb:KYW planar waveguide laser Q-switched by evanescent-field interaction with carbon nanotubes," Opt. Lett. **38**(23), 5090–5093 (2013).
11. J. W. Kim, S. Young Choi, S. Aravazhi, M. Pollnau, U. Griebner, V. Petrov, S. Bae, K. Jun Ahn, D.-I. Yeom, and F. Rotermund, "Graphene Q-switched Yb:KYW planar waveguide laser," AIP Adv. **5**(1), 017110 (2015).
12. Y. Tan, C. Cheng, S. Akhmadaliev, S. Zhou, and F. Chen, "Nd:YAG waveguide laser Q-switched by evanescent-field interaction with graphene," Opt. Express **22**(8), 9101–9106 (2014).
13. Y. Tan, R. He, J. Macdonald, A. K. Kar, and F. Chen, "Q-switched Nd:YAG channel waveguide laser through evanescent field interaction with surface coated graphene," Appl. Phys. Lett. **105**(10), 101111 (2014).
14. H. Liu, C. Cheng, C. Romero, J. R. Vázquez de Aldana, and F. Chen, "Graphene-based Y-branch laser in femtosecond laser written Nd:YAG waveguides," Opt. Express **23**(8), 9730–9735 (2015).
15. L. Ma, Y. Tan, S. Akhmadaliev, S. Zhou, and F. Chen, "Electrically Tunable Nd:YAG waveguide laser based on Graphene," Sci. Rep. **6**(1), 36785 (2016).
16. A. Choudhary, S. J. Beecher, S. Dhingra, B. D'Urso, T. L. Parsonage, J. A. Grant-Jacob, P. Hua, J. I. Mackenzie, R. W. Eason, and D. P. Shepherd, "456-mW graphene Q-switched Yb:yttria waveguide laser by evanescent-field interaction," Opt. Lett. **40**(9), 1912–1915 (2015).
17. Y. Tan, Z. Guo, L. Ma, H. Zhang, S. Akhmadaliev, S. Zhou, and F. Chen, "Q-switched waveguide laser based on two-dimensional semiconducting materials: tungsten disulfide and black phosphorous," Opt. Express **24**(3), 2858–2866 (2016).
18. E. Kifle, X. Mateos, P. Loiko, S. Y. Choi, J. E. Bae, F. Rotermund, M. Aguiló, F. Díaz, U. Griebner, and V. Petrov, "Tm:$KY_{1-x-y}Gd_xLu_y(WO_4)_2$ planar waveguide laser passively Q-switched by single-walled carbon nanotubes," Opt. Express **26**(4), 4961–4966 (2018).
19. S. Y. Choi, T. Calmano, F. Rotermund, and C. Kränkel, "2-GHz carbon nanotube mode-locked Yb:YAG channel waveguide laser," Opt. Express **26**(5), 5140–5145 (2018).
20. M. Pollnau, Y. E. Romanyuk, F. Gardillou, C. N. Borca, U. Griebner, S. Rivier, and V. Petrov, "Double tungstate lasers: From bulk toward on-chip integrated waveguide devices," IEEE J. Sel. Top. Quant. **13**(3), 661–671 (2007).
21. Y. E. Romanyuk, C. N. Borca, M. Pollnau, S. Rivier, V. Petrov, and U. Griebner, "Yb-doped $KY(WO_4)_2$ planar waveguide laser," Opt. Lett. **31**(1), 53–55 (2006).
22. F. Gardillou, Y. E. Romanyuk, C. N. Borca, R.-P. Salathé, and M. Pollnau, "Lu, Gd codoped $KY(WO_{(4)})_2$:Yb epitaxial layers: towards integrated optics based on $KY(WO_4)_2$," Opt. Lett. **32**(5), 488–490 (2007).

Optics EXPRESS

23. D. Geskus, S. Aravazhi, C. Grivas, K. Wörhoff, and M. Pollnau, "Microstructured $KY(WO_4)_2$:Gd^{3+}, Lu^{3+}, Yb^{3+} channel waveguide laser," Opt. Express **18**(9), 8853–8858 (2010).
24. D. Geskus, S. Aravazhi, E. Bernhardi, C. Grivas, S. Harkema, K. Hametner, D. Günther, K. Wörhoff, and M. Pollnau, "Low-threshold, highly efficient Gd^{3+}, Lu^{3+} co-doped $KY(WO_4)_2$:Yb^{3+} planar waveguide lasers," Laser Phys. Lett. **6**(11), 800–805 (2009).
25. W. Bolaños, J. J. Carvajal, X. Mateos, G. S. Murugan, A. Z. Subramanian, J. S. Wilkinson, E. Cantelar, D. Jaque, G. Lifante, M. Aguiló, and F. Díaz, "Mirrorless buried waveguide laser in monoclinic double tungstates fabricated by a novel combination of ion milling and liquid phase epitaxy," Opt. Express **18**(26), 26937–26945 (2010).
26. W. Bolaños, J. J. Carvajal, M. Cinta Pujol, X. Mateos, G. Lifante, M. Aguiló, and F. Díaz, "Epitaxial growth of lattice matched $KY_{1-x-y}Gd_xLu_y(WO_4)_2$ thin films on $KY(WO_4)_2$ substrates for waveguiding applications," Cryst. Growth Des. **9**(8), 3525–3531 (2009).
27. O. Silvestre, A. Aznar, R. Solé, M. C. Pujol, F. Díaz, and M. Aguilo, "Lattice mismatch and crystal growth of monoclinic $KY_{1-x}Yb_x(WO_4)_2/KY(WO_4)_2$ layers by liquid phase epitaxy," J. Phys. Condens. Matter **20**(22), 225004 (2008).
28. J. H. Yim, W. B. Cho, S. Lee, Y. H. Ahn, K. Kim, H. Lim, G. Steinmeyer, V. Petrov, U. Griebner, and F. Rotermund, "Fabrication and characterization of ultrafast carbon nanotube saturable absorbers for solid-state laser mode locking near 1 μm," Appl. Phys. Lett. **93**(16), 161106 (2008).
29. A. S. Yasukevich, P. Loiko, N. V. Gusakova, J. M. Serres, X. Mateos, K. V. Yumashev, N. V. Kuleshov, V. Petrov, U. Griebner, M. Aguiló, and F. Díaz, "Modelling of graphene Q-switched Tm lasers," Opt. Commun. **389**, 15–22 (2017).